Meanwhile, boundary conditions at $x = 1$ are obtained by imposing flatness at spatial infinity:

$$F_0 = F_1 = F_2 = \phi = A_\varphi = A_t - \Phi = W = 0. \tag{14}$$

On the symmetric axis, axial symmetry and regularity impose the following conditions at $\theta = 0$ and $\theta = \pi$:

$$\partial_\theta F_0 = \partial_\theta F_1 = \partial_\theta F_2 = \partial_\theta \phi = \partial_\theta A_\varphi = \partial_\theta A_t = \partial_\theta W = 0. \tag{15}$$

In this work, we focus on solutions exhibiting equatorial-plane symmetry, allowing us to restrict the computational domain to the upper half-plane $0 \leq \theta \leq \pi/2$. Consequently, the $\theta = \pi$ boundary condition in Eq. (15) is replaced with

$$\partial_\theta F_0 = \partial_\theta F_1 = \partial_\theta F_2 = \partial_\theta \phi = \partial_\theta A_\varphi = \partial_\theta A_t = \partial_\theta W = 0 \text{ at } \theta = \pi/2. \tag{16}$$

Consequently, Eqs. (13), (14), (15) and (16) serve as the boundary conditions for solving the partial differential equations. Additionally, the absence of conical singularities imposes $F_1 = F_2$ on the symmetry axis, which provides an independent consistency check for our numerical results alongside the Smarr relation [31, 58].

This work employs spectral methods to numerically solve the coupled nonlinear partial differential equations governing the system. Spectral methods are well-established and particularly effective for solving nonlinear elliptic partial differential equations. They approximate solutions using a finite linear combination of basis functions, thereby transforming the differential equations into a system of algebraic equations. A key advantage of spectral methods is their exponential convergence rate with increasing resolution, which far exceeds the linear or polynomial convergence characteristic of finite difference or finite element methods.

In our numerical work, we implement spectral methods by approximating the functions of interest, collectively denoted by $\mathcal{F} = \{F_0, F_1, F_2, W, A_t, A_\varphi, \phi\}$, as a finite linear combination of basis functions:

$$\mathcal{F}^{(k)} = \sum_{i=0}^{N_x-1} \sum_{j=0}^{N_\theta-1} a_{ij}^{(k)} T_i(x) \cos(2j\theta), \tag{17}$$

where $T_i(x)$ represents the i-th Chebyshev polynomial, $a_{ij}^{(k)}$ are the spectral coefficients, and N_x and N_θ denote the resolutions in the radial and angular coordinates, respectively. To determine $\alpha_{ij}^{(k)}$, we substitute the spectral expansions (17) into the equations of motion and then discretize the resulting equations at the Gauss-Chebyshev points. This process transforms the partial differential equations for $\mathcal{F}^{(k)}$ into a finite system of algebraic equations for $a_{ij}^{(k)}$. These algebraic equations

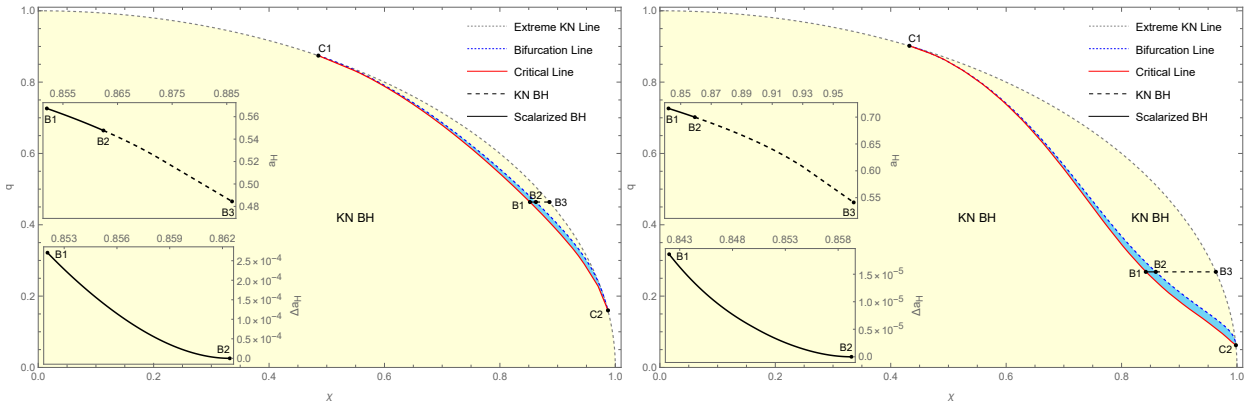

FIG. 1. Domain of existence for spin-induced scalarized KN black holes in the (χ, q) parameter space. **Left Panel:** $\alpha = -100$. **Right Panel:** $\alpha = -1000$. The light yellow region indicates the parameter space of KN black holes, bounded by the extremal KN line corresponding to $q^2 + \chi^2 = 1$. The light blue region denotes the domain of existence for scalarized black holes, within which both KN and scalarized solutions coexist. This domain is bounded by the bifurcation line (blue dashed), where scalarized black holes branch off from KN black holes, and the critical line (red solid), beyond which scalarized black holes can no longer be obtained numerically. Toward both ends of the existence domain, the extremal KN line, bifurcation line and critical line converge and merge at the critical points C_1 and C_2. The marked points B_1, B_2 and B_3 on constant-q lines represent a critical scalarized black hole, a bifurcating KN black hole and an extremal KN black hole, respectively. The upper inset shows the reduced horizon area a_H as a function of χ along the constant-q line connecting B_1 and B_3. The lower inset displays Δa_H, the difference in a_H between KN and scalarized black holes, also as a function of χ. The black dashed line traces KN black hole solutions, while the black solid line corresponds to scalarized black holes.

are then solved using the Newton-Raphson method, with the root-finding process carried out using Mathematica's built-in LinearSolve function.

III. NUMERICAL RESULTS

In this section, we first identify the domain of existence for spin-induced scalarized KN black holes and subsequently analyze their properties. As previously discussed, stationary scalar clouds around KN black holes emerge for $\alpha < 0$ when the black hole spin exceeds a critical threshold. Consequently, we focus on the $\alpha < 0$ regime to construct spin-induced scalarized solutions. For the coupling function, we employ the exponential form $f(\phi) = e^{\alpha\phi^2}$ throughout this section. For comparison, a quadratic coupling function $f(\phi) = 1+\alpha\phi^2$ is examined in Appendix B. Additionally, we restrict our attention to fundamental black hole solutions, characterized by a nodeless scalar field.

In Appendix A, we conduct convergence tests of scalarized black hole solutions by monitoring the Smarr relation and the absence of conical singularities for varying resolutions, N_x or N_θ. As anticipated, the convergence tests demonstrate exponential convergence as the resolution increases, persisting until a roundoff plateau is reached. To ensure numerical precision and efficiency, we employ spectral methods with resolutions $N_x = 40$ and $N_\theta = 11$ to solve the partial differential equations. With these resolutions, our results indicate that the numerical error of scalarized black hole solutions is less than 10^{-8} when they are sufficiently distant from the critical line. However, as we approach the critical line, the solutions exhibit a numerical error on the order of 10^{-5}. For convenience, we introduce dimensionless reduced quantities $q \equiv Q/M$, $\chi \equiv J/M^2$ and $a_H \equiv A_H/16\pi M$ in the remainder of this section.

Fig. 1 displays the domain of existence for spin-induced scalarized KN black holes in the (χ, q) parameter space, with $\alpha = -100$ (left panel) and $\alpha = -1000$ (right panel). The light blue region, bounded by the bifurcation and critical lines, marks the parameter space where scalarized black holes exist. The bifurcation line corresponds to the threshold at which the tachyonic instability triggers the formation of stationary scalar cloud around KN black holes. Both endpoints, C_1 and C_2, of the bifurcation line lie on the extremal KN black hole line, defined by $q^2 + \chi^2 = 1$. Starting from the bifurcation line, scalarized black hole solutions are computed along constant-χ lines by varying q until reaching the critical line. Beyond this line, numerical solutions cannot be reliably obtained with an error below 10^{-5}. Interestingly, our numerical results show that the critical line asymptotically approaches both endpoints of the bifurcation line, implying that the bifurcation and critical lines merge at C_1 and C_2. This indicates that spin-induced scalarized KN black holes do not exist when the spin is either too low or too high. Furthermore, Fig. 1 illustrates that the existence domain expands as $|\alpha|$ increases.

As shown in [55], KN black holes below the bifurcation line are stable against the scalar perturbation, while those above exhibit a tachyonic instability. Therefore, Fig. 1 demonstrates that spin-induced scalarized KN black holes coexist with stable KN black holes possessing the same q and χ within their domain of existence. To examine the behavior of the horizon area, we highlight three distinct black hole configurations with the same q in Fig. 1: B_1, a critical scalarized black hole; B_2, a black hole on the bifurcation line; B_3, an extremal KN black hole. The upper insets show that the reduced horizon area a_H of scalarized black holes decreases as the spin increases for fixed q. The lower insets display Δa_H, the difference in reduced horizon area between KN and scalarized black holes, along the constant-q line connecting B_1 and B_2. These results indicate that KN black holes generally have a larger reduced horizon area than scalarized black holes with the